



1 The ST22 chronology for the Skytrain Ice Rise ice core - part 2: an age model to the last interglacial
2 and disturbed deep stratigraphy.

3 **Authors:** Robert Mulvaney¹, Eric W. Wolff², Mackenzie M. Grieman^{2,3}, Helene H. Hoffmann², Jack D.
4 Humby¹, Christoph Nehrbass-Ahles², Rachael H. Rhodes², Isobel F. Rowell², Frédéric Parrenin⁴, Loïc
5 Schmidely⁵, Hubertus Fischer⁵, Thomas F. Stocker⁵, Marcus Christl⁶, Raimund Muscheler⁷, Amaelle
6 Landais⁸, Frédéric Prié⁸

7

8 1. British Antarctic Survey, Cambridge, UK

9 2. Department of Earth Sciences, University of Cambridge, UK

10 3. Reed College, Portland, Oregon, USA

11 4. Université Grenoble Alpes, CNRS, IRD, Grenoble INP, IGE, 38000 Grenoble, France

12 5. Climate and Environmental Physics, Physics Institute, and Oeschger Centre for Climate Change
13 Research, University of Bern, Switzerland

14 6. Laboratory for Ion Beam Physics, ETH Zurich, 8093 Zurich, Switzerland

15 7. Department of Geology, Quaternary Sciences, Lund University, Sölvegatan 12, SE-22362 Lund,
16 Sweden

17 8. Laboratoire des Sciences du Climat et de l'Environnement, LSCE/IPSL, CEA-CNRS-UVSQ, Université
18 Paris-Saclay, Gif-sur-Yvette, France

19 Correspondence to: Eric Wolff (ew428@cam.ac.uk)

20

21 1. Abstract

22 We present an age model for the 651 m deep Skytrain Ice Rise ice core. The top 2000 years have
23 previously been dated using age markers interpolated through annual layer counting. Below this, we
24 align the Skytrain core to the AICC2012 age model using tie points in the ice and air phase, and apply
25 the Paleochrono program to obtain the best fit to the tie points and glaciological constraints. In the
26 gas phase, ties are made using methane and, in critical sections, $\delta^{18}\text{O}_{\text{air}}$; in the ice phase ties are
27 through ^{10}Be across the Laschamps Event, and through ice chemistry related to long-range dust
28 transport and deposition. This strategy provides a good outcome to about 108 ka (~605 m). Beyond
29 that there are signs of flow disturbance, with a section of ice probably repeated. Nonetheless values
30 of CH_4 and $\delta^{18}\text{O}_{\text{air}}$ confirm that part of the last interglacial (LIG), from about 117-126 ka (617-628 m),
31 is present and in chronological order. Below this there are clear signs of stratigraphic disturbance,
32 with rapid oscillation of values in both the ice and gas phase at the base of the LIG section. Based on



33 methane values, the warmest part of the LIG and the coldest part of the penultimate glacial are
34 missing from our record. Ice below 631 m appears to be of age >150 ka.

35

36 2. Introduction

37

38 There is currently intense interest in the role of the Antarctic Ice Sheet, and the West Antarctic Ice
39 Sheet (WAIS) in particular, in future sea level rise (DeConto et al., 2021; Fox-Kemper et al., 2021).
40 While modern studies of the behaviour of the WAIS are essential, studies aimed at assessing the past
41 stability of the WAIS and its response to past climate change are required to constrain the operation
42 of proposed feedbacks (such as the Marine Ice Cliff Instability mechanism) (Gilford et al., 2020). The
43 last interglacial (LIG, Marine Isotope Stage (MIS) 5e, ~130-110 ka before present (bp) where present
44 is defined as 1950) has been considered of particular interest because estimates of sea level during
45 that period compared to the present (Dutton et al., 2015; Dyer et al., 2021) appear to require some
46 contribution from retreat of the Antarctic Ice Sheet. In order to assess the sensitivity of the WAIS
47 and its surrounds to climate change, it is also of interest to understand how the climate and the ice
48 in the WAIS region responded to the coolings and warmings of the last glacial period and the
49 warming into the Holocene.

50 While there are a number of Antarctic ice core records extending through at least one climate cycle
51 and into the LIG from East Antarctica (e.g. Crotti et al., 2021; EPICA Community Members, 2004;
52 Grootes et al., 2001; Kawamura et al., 2007), long records from West Antarctica are scarce. The
53 WAIS Divide ice core (Fig. 1) provides an excellent and well-resolved record of the last 68 kyr (Buizert
54 et al., 2015) but does not extend further back in time. The only other long core in the interior of the
55 WAIS is the 2191 m long Byrd core, for which the oldest ages presented are 90 ka (Ahn and Brook,
56 2008). On the periphery of the WAIS, the Siple Dome core reached the bed at 1004 m, but again data
57 have only been presented as far back as 90 ka (Brook et al., 2005; Saltzman et al., 2006). At
58 Roosevelt Island, situated within the Ross Ice Shelf, the ice could not yet be dated beyond 83 ka (Lee
59 et al., 2020). Old ice might be available at the bottom of the Berkner Island (Mulvaney et al., 2007)
60 and Fletcher Promontory (Mulvaney et al., 2014) cores, but there is no published age scale for these
61 cores so far.



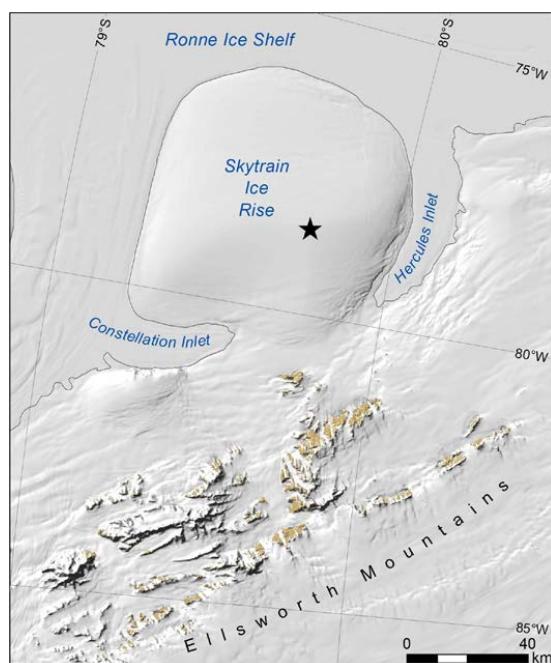
62

63 Figure 1. Map showing ice core sites in West Antarctica that are mentioned in text. Map generated
64 using QGIS with the Quantarctica mapping environment (Matsuoka et al., 2021).

65 The only record that seems to unequivocally reach the LIG in West Antarctica to date is that from a
66 horizontal ice trench in the blue ice area at Mount Moulton (Korotkikh et al., 2011). This appears to
67 reach 135 ka, although the nature of the record makes it hard to assess its continuity. It is therefore
68 a priority to find sites in the WAIS vicinity where a record extending to the LIG can be retrieved and
69 fully analysed. One potential candidate site, near the boundary between the East and West Antarctic
70 Ice Sheets, would be Hercules Dome (Jacobel et al., 2005), and drilling is expected there in the next
71 few years. In this paper we present an age scale for an ice core drilled at Skytrain Ice Rise, at the
72 boundary of the WAIS and the Ronne Ice Shelf.



73 The core at Skytrain Ice Rise was drilled to the bed at 651 m depth in 2018-19 (Mulvaney et al.,
74 2021). Skytrain Ice Rise (Fig. 2) is an independent ice rise (i.e., with its own flow regime) with a
75 circular shape and a diameter of ~80 km. It sits at an altitude of 784 m, has a 10 m temperature
76 (representing mean annual temperature today) of -25.9°C, and a basal temperature of -14.9°C. It
77 represents an attractive target because it's isotopic and chemical content should be sensitive to
78 changes in the extent and altitude of the WAIS, and also to the extent of the adjacent Ronne Ice
79 Shelf. It is situated on a bed that is above sea level, but surrounded almost entirely by ice shelf
80 (including Constellation and Hercules Inlets, see Fig. 2) that has a sea bed depth of at least 1000 m.
81 On the WAIS side, it is protected by the Ellsworth Mountains. This combination ensures that Skytrain
82 Ice Rise will almost certainly have remained as a separate ice dome, and would never have been
83 overridden by inland ice, whatever the size of the WAIS.



84

85 Figure 2. Skytrain Ice Rise. The drill site is marked with a star. Figure reproduced from (Mulvaney et
86 al., 2021), [CC BY 4.0](https://creativecommons.org/licenses/by/4.0/)

87 Radar data collected previously (J. Kingslake, pers. comm.) showed good layering almost to the bed
88 (Mulvaney et al., 2021), with a pronounced Raymond Arch. The drill site was chosen based on the
89 radar layers to give old ice as far from the bed as possible.



90 In a companion paper to this one (Hoffmann et al., 2022) we have used a variety of age markers,
91 interpolated through counting of annual layers in chemistry, to derive an age scale for the last 2000
92 years (~200 m). In this paper we use a range of evidence to derive an age model for the rest of the
93 core. In particular, we demonstrate that the core contains an intact record of the last glacial period
94 and extends into the LIG. We also discuss the possible age of more disturbed ice found in the
95 deepest twenty metres of the core.

96

97 3. Overall dating strategy

98 The strategy, as with other recent dating papers (Epifanio et al., 2020), is to tie the Skytrain Ice Rise
99 core to a well-established age model. Since we expected our core to run well beyond the age of the
100 WAIS Divide core, we have chosen to give our final derived ages as those of the AICC2012 age model
101 (Bazin et al., 2013; Veres et al., 2013), which was developed for the EPICA ice cores but includes
102 synchronized age scales for some of the major East Antarctic Ice Sheet deep ice cores (Talos Dome,
103 Vostok) and which is synchronized to the Greenland NGRIP ice core in the upper 60 kyr. However,
104 we recognise that the WD2014 age model (Buizert et al., 2015; Sigl et al., 2016), developed for the
105 WAIS Divide ice core) is more accurate in absolute age over the last 68 kyr, and that methane data
106 are available at a much higher resolution in cores that have been tied to it. For that reason, in some
107 cases we initially matched our core to WD2014 and then used a simple translation table to tie it to
108 AICC2012. For convenience, our depth-age table in the supplement provides both WD2014 and
109 AICC2012 ages for the last 68 kyr. This is based on volcanic synchronisations (Buizert et al., 2018; Sigl
110 et al., 2022) for the age of the ice.

111 In order to construct the age alignment, and estimate uncertainty, we use the Paleochrono program
112 which is a development of the Icechron program (Parrenin et al., 2015). We include a number of
113 stratigraphic alignments to AICC2012, based on the data in the companion paper for the uppermost
114 2000 years, and using CH₄, δ¹⁸O_{air}, ¹⁰Be, and ice chemistry markers in deeper ice. Paleochrono was
115 started with a prior for the accumulation rate (based on a simple relationship with water isotope
116 ratios), air lock-in depth (prior set at a constant 58 m (Hoffmann et al., 2022)) and a simple ice
117 thinning function. Paleochrono minimises a cost function that measures the misfit of the model with
118 respect to the prior and the observations (tie points).

119 3.1. Flow disturbance

120 In the deeper part of the ice core, between 628-635 m, we observe some discontinuities, with rapid
121 and simultaneous changes in water isotopes and methane at the same depth. These will be



122 discussed in more detail later, but they represent likely depths of flow disturbance or folding, as has
123 been observed in other ice core records, including those of the LIG in Greenland (Chappellaz et al.,
124 1997; NEEM Community Members, 2013; Yau et al., 2016). We also deduce that some disturbance
125 may exist in a region between about 605 and 615 m depth. From 600 m downwards we therefore
126 carefully examine individual data points (using paired values of CH₄ and δ¹⁸O_{atm} matched against
127 reference data) to reconstruct discrete ages for particular depths. This allows us to assess which
128 sections are in order with well-constrained ages, and which are disturbed in the deeper ice. We then
129 use Paleochrono to derive a continuous age model to 630 m, making manual adjustments to the
130 final age scale to avoid assigning spurious ages to data in the disturbed section.

131

132 4. Data available

133

134 In this section we describe the collection of the data used to make ties to other cores, both in the
135 gas phase (air bubbles) and in the ice phase.

136

137 4.1. Continuous methane

138 Methane measurements are a particularly powerful way of aligning the gas ages of different ice
139 cores because they exhibit large (from tens to 200 ppb) and abrupt changes of concentration across
140 millennial-scale Dansgaard-Oeschger events that recur throughout the last glacial period (e.g.
141 Epifanio et al., 2020). Using high-resolution continuous analysis it has also been shown that
142 centennial and faster variability down to below 10 ppb amplitude is well-reproduced between cores
143 (Lee et al., 2020; Mitchell et al., 2013; Rhodes et al., 2017). As methane is well-mixed in the Antarctic
144 troposphere, not just the pattern but the absolute values should match with reference datasets
145 within uncertainty. Our main dataset, the continuous one from CFA, is good at showing the high-
146 resolution variability, but has a large and unknown uncertainty in absolute values. We therefore
147 supplement it with some discrete analyses (section 4.2) that constrain the concentration tightly at
148 key sections of ice.

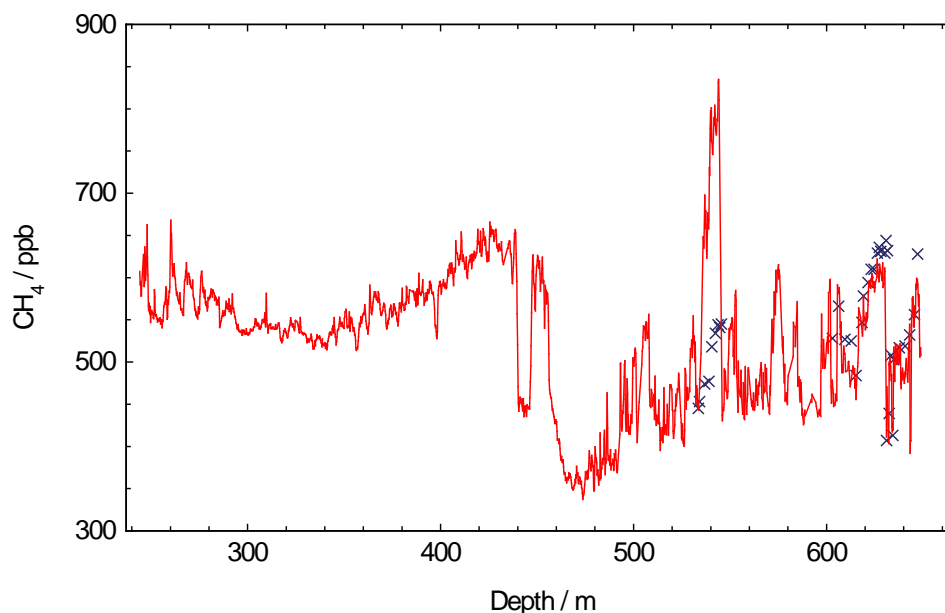
149 We measured methane (CH₄) continuously during the continuous flow analysis (CFA) campaign
150 (Grieman et al., 2021). Briefly, the core was melted at a mean rate of 3.2 cm min⁻¹ and the air was
151 separated from residual water flow using a 3M Liqui-Cel MM-0.5x1 Series membrane contactor. The
152 dried air was then directed to a Picarro G2301 CRDS for CH₄ analysis. While the methane Picarro
153 calibration could not be checked against external certified standards, comparison of our data



154 produced by CFA with analysis of discrete samples analysed in Bern (section 4.2), as well as
155 comparison of our CFA data with reference data across the Holocene and glacial, suggests that the
156 CFA methane reproduces the variability in methane at centennial scales. However, the absolute
157 values are offset (mainly low) by an amount that varied by a few percentage points over the
158 campaign but the offset was typically below 10%. This offset arises partly from dissolution of a small
159 percentage of gas into the meltwater stream, as has been observed previously using CFA to measure
160 methane (Rhodes et al., 2015). Continuous analyses started at 244 m depth and continued in all
161 sections where the ice was of suitable quality to 649.4 m. A short section from 144.0-161.3 m was
162 also analysed continuously for methane with an improved measurement setup which is discussed in
163 the companion paper (Hoffmann et al., 2022).

164 Two significant issues affected the measurements. Firstly, a section of data between 534 and 545 m
165 was affected by a leak of lab air at the membrane contactor. The absolute values in this section of
166 ice are therefore substantially higher than palaeoatmosphere, but the pattern of variability can still
167 partly be used for wiggle-matching after correction using discrete analyses (next section).

168 A second issue is that there were increasing numbers of breaks and cracks in the ice with depth,
169 particularly below 450 m. Badly cracked sections were removed before the ice was placed on the
170 melter and breaks across the core were smoothed with a cleaned file to ensure that the contact
171 between ice sections was as close as possible. With these precautions, such occurrences do not
172 affect the ice phase chemical measurements and most do not affect CH₄ either. Nonetheless some of
173 the remaining cracks and transitions between different bags provide an opportunity for the ingress
174 of lab air as the ice melts, leading to spikes in methane concentration. Major short peaks and
175 troughs were identified using the "ginput" MATLAB function, and removed from the dataset. Above
176 500 m ~25 spikes that were at least a factor 2 higher or lower than the mean of the dataset were
177 removed. Below 500 m, the data became much noisier and ~100 deviations from the dataset were
178 manually removed. Even after removal of the obvious spike artefacts the data remain more noisy
179 than the data that are unaffected by such artefacts, suggesting that positive artefacts arising from
180 inclusion of modern air remain in the dataset. This makes it trickier to clearly align data with a
181 reference dataset in the deeper ice. The dataset below 244 m is shown in Fig 3.



182
183 Figure 3. Continuous (CFA) methane (red), and data from discrete measurements (black crosses),
184 after removal of occasional methane spikes as discussed in the text. The discrete data confirm that
185 the continuous data between 534 and 545 m are offset, and confirm that the uncalibrated values for
186 the remaining continuous data are reasonable.

187 4.2. Discrete methane

188 To validate and control that the absolute levels of our continuous CH₄ record are consistent within
189 uncertainty with the absolute values in reference data, we obtained some well-calibrated discrete
190 measurements (Fig. 3), particularly in the deep ice and in the section impacted by the air leak
191 (section 3.1). Ten discrete samples were therefore measured at the University of Bern between 533-
192 546 m, and a further 25 samples between 600 and 650 m depth. Details of the method have been
193 published elsewhere (Schmidely et al., 2021). Concentrations ranged between 413 and 644 ppb,
194 with an estimated precision (1 sigma) of 7 ppb (Table S1). Note that the discrete data presented here
195 have been corrected by -18 ppb (Schmidely et al., 2021) to align them with previously published CH₄
196 records. These offsets are potentially due to different remnant solubility of CH₄ in meltwater using
197 different melt extraction methods in different labs. Taking the uncertainty of the correction into
198 account, the total uncertainty is estimated at 12 ppb (Schmidely et al., 2021), while that of the
199 reference data is estimated at 10 ppb (Loulergue et al., 2008). Combining these uncertainties
200 suggests that when comparing absolute values of methane (discrete data) with reference datasets
201 we should allow an uncertainty of 16 ppb (much higher offsets are possible for the data derived by



202 CFA, and there we mainly look for similar patterns to those in the reference data). The discrete data
203 measured in Bern are displayed along with the continuous data in Fig. 3. A number of discrete
204 measurements were also made between 84 and 144 m at Oregon State University which are
205 described in the companion paper (Hoffmann et al., 2022).

206 4.3. $\delta^{18}\text{O}$ of O_2 ($\delta^{18}\text{O}_{\text{atm}}$)

207 The isotopic ratio of oxygen in air provides a good additional constraint because it is well-mixed
208 globally, and varies in line with precession, providing opportunities for aligning measurements with
209 calculated orbital targets as well as with measurements from other ice cores (Extier et al., 2018).
210 CH_4 and $\delta^{18}\text{O}_{\text{atm}}$ have previously been used powerfully in tandem to untangle disturbed ice
211 chronologies in the LIG (Chappellaz et al., 1997; Yau et al., 2016).

212 In this work, 27 samples were analysed for $\delta^{18}\text{O}_{\text{atm}}$ at the Laboratoire des Sciences du Climat et de
213 l'Environnement (LSCE). Two samples were in the depth range 160-170 m, and 5 were between 435
214 and 471 m. The remaining samples were in the depth range 602-635 m. Data were corrected for firn
215 fractionation and gas loss (Extier et al., 2018) and are shown in Table S1. Uncertainty on each value
216 is estimated at +/- 0.03 ‰. Combining this with the similar uncertainty in data points in the
217 reference dataset suggests that we should allow an uncertainty of 0.04‰ when comparing our data
218 with the reference.

219 4.4. ^{10}Be across the Laschamps Event

220 The flux/concentration of ^{10}Be in ice shows a pattern related to variations in the magnetic field of
221 the Sun and, on longer timescales, Earth. The pattern of these variations can be matched between
222 ice cores, and with ^{14}C variations in other archives such as tree rings, in order to synchronise records
223 (e.g. Adolphi and Muscheler, 2016). A particularly clear and prominent pattern is seen across the
224 Laschamps Event, a weakening of Earth's magnetic field that occurred around 41 ka bp (e.g. Raisbeck
225 et al., 2017). Because this section of ice is in the last glacial period, its synchronisation in the ice
226 phase should allow for a particularly useful and unambiguous estimate of the offset between ice age
227 and gas age (Δage) in the glacial period.

228 Seventy samples from between 509 and 520 m depth were spiked with a known amount of ^9Be ,
229 processed in Lund and analysed for ^{10}Be by Accelerator Mass Spectrometry at ETH Zurich. Measured
230 $^{10}\text{Be}/^9\text{Be}$ ratios were normalized to the ETH Zurich in-house standards S2007N and S2010N with
231 nominal $^{10}\text{Be}/^9\text{Be}$ ratios of 28.1×10^{-12} and 3.3×10^{-12} (Christl et al., 2013). Data and associated
232 uncertainties are presented in Table S2.

233 4.5. Aluminium (Al) and non sea salt magnesium (nssMg)



234 When synchronising ice cores from different sites, it is important to use only parameters for which
235 there is a sound reason to assume that both cores share synchronous variability. This is the case, for
236 example, with volcanic eruption spikes, with ^{10}Be and with well-mixed atmospheric gases, such as
237 methane. It is not safe to make such an assumption for water isotopes, which are site-dependent
238 because climatic changes may vary asynchronously in different parts of Antarctica. While methane
239 synchronisation (see above) and a relatively small Δage compared to inland sites (due to the higher
240 accumulation rate) allows us to make a reasonable estimate of the ice age along our core, it would
241 be advantageous to have further ties in the ice phase. It has been argued previously that variations
242 in the components of terrestrial dust (such as Ca) can be assumed to be synchronous across
243 Antarctica (Baggenstos et al., 2018; Mulvaney et al., 2000). This is because their concentrations are
244 strongly controlled by events at a common source in South America and in a common part of the
245 transport pathway towards Antarctica, with only a minor part of the variability likely to be
246 dependent on the final stages of transport to each ice core site.

247 The main component used for such synchronisation to date has been non-sea-salt (nss) Ca,
248 calculated using marine and terrestrial ratios of Ca and Na (e.g. Röthlisberger et al., 2002)). However,
249 after an initial attempt we observed that while nssCa at Skytrain Ice Rise shows a good coherence
250 with that of other sites (EDC, EDML) until a depth of about 500 m (30 ka bp), it diverges below that.
251 Other terrestrial markers such as Al and nssMg (calculated as $\text{Mg}-0.12*\text{Na}$ and both measured by
252 ICP-MS during the CFA campaign (Grieman et al., 2021)) do not mirror the Skytrain nssCa signal, and
253 do appear to follow nssCa at other East Antarctic sites (see section 6.3). It appears that an additional
254 source of Ca-rich material, not seen in other Antarctic cores and presumably due to local sources, is
255 present at this site in the earlier part of the last glacial. The reasons for this will be explored
256 elsewhere. However, the solution for us is to use the terrestrial markers that appear free from this
257 extra source, but that are coherent with nssCa records at other sites. The limits of detection of Al
258 and Mg are 3.3 ppb and 1.3 ppb, respectively. We concentrate on alignments from nssMg because a
259 majority of Al values in the Holocene and marine isotope stage 5 fall below the detection limit; in the
260 glacial the Al values support our conclusions with nssMg.

261 5. Reference datasets

262 Since the basis for our age model is tying variations in our data to variations in well-dated ice cores,
263 in this section we describe the reference datasets used.

264 5.1. Gas phase: Methane and $\delta^{18}\text{O}$ of O_2 ($\delta^{18}\text{O}_{\text{atm}}$)



265 In order to use the more detailed variability that can be traced during the Holocene, we compared
266 our methane data to the high resolution Roosevelt Island methane record between 2-7 ka bp.
267 Between 7-68 ka we used the WAIS Divide record (Buizert et al., 2015; Rhodes et al., 2017). Between
268 68 and 156 ka, we used the southern hemisphere methane spline generated from the EDC ice core
269 (Köhler et al., 2017). To investigate possible matches with older ice we used the EDC data itself
270 (Loulergue et al., 2008). As previously explained, the Roosevelt and WAIS Divide data are on the
271 WD2014 age scale, but we eventually used a conversion table (based on Buizert et al., 2018) to place
272 all matches onto a common AICC2012 age scale.

273 A composite EDC-Vostok record of $\delta^{18}\text{O}_{\text{atm}}$ (Extier et al., 2018) was used for comparison to Skytrain
274 ice core $\delta^{18}\text{O}_{\text{atm}}$.

275 5.2. Ice phase: ^{10}Be across the Laschamps Event and terrestrial marker elements

276 The clear pattern of the ^{10}Be record across the Laschamps Event has been shown to be closely
277 replicated at several sites in Greenland and Antarctica (Raisbeck et al., 2017). For the
278 synchronisation, we used the normalised stack that was recently created based on 3 Greenland and
279 3 Antarctic records (Adolphi et al., 2018).

280 As the reference dataset for terrestrial deposition we used the nssCa record from EDML (Fischer et
281 al., 2007), because of its greater proximity to Skytrain in the Atlantic sector of Antarctica, with
282 further validation using the record from EDC (Wolff et al., 2010).

283 6. Tie points to 100 ka

284 6.1. Methane

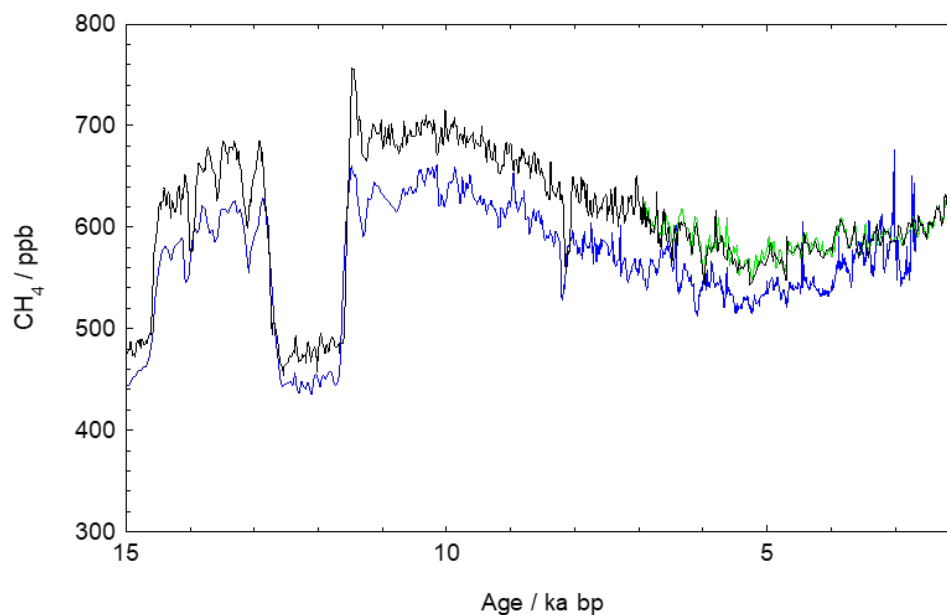
285 First, we note that the discrete methane data (Fig. 3) confirm that the methane concentrations in
286 the section from 534-545 m are much too high. In this section of ice we therefore use the values
287 from the discrete data to match with reference data.

288 In Table S3, we list the methane tie points that we used in this section. The very clear match
289 between our record and the reference data is ideally seen in the past 15 kyr (460 m) where there are
290 few spikes in the methane record due to air ingress into cracks (Fig. 4). However, the pattern of
291 Dansgaard-Oeschger events remains clear right down to 100 ka, and is shown in Fig. 5, along with
292 the tie points used. We note that the comparisons in Fig. 4 suggest that the Skytrain data might be
293 up to 10% too low in concentration (but with a variable offset along the core) compared to the
294 reference data; this results from the dissolution of gas in the meltstream (as discussed in section 4.1)
295 and the difficulty of accurately calibrating data from the continuous melter due to the absence of an
296 external certified standard. In Fig. 5 we show the full methane record on the eventual age scale,



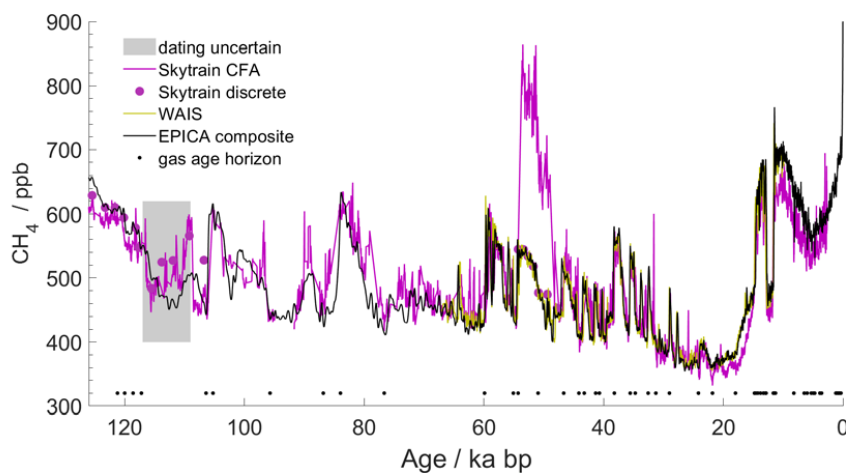
297 compared to reference data. It is clear that some spikes due to air ingress across cracks remain in the
298 dataset beyond about 60 ka, but the pattern for matching is still apparent to at least 100 ka. The
299 section beyond 100 ka will be discussed in section 7.

300



301

302 Figure 4. Methane matching over the last 15 kyr. Methane from Skytrain Ice Rise (blue) on its age
303 scale after synchronisation, along with methane from Roosevelt Island (green) (Lee et al., 2020), and
304 WAIS Divide (black) (Buizert et al., 2015; Mitchell et al., 2013). Ages shown here are WD2014. The
305 concentration offset between the Skytrain and other data is probably caused by partial dissolution in
306 the meltstream for Skytrain as discussed in the text.

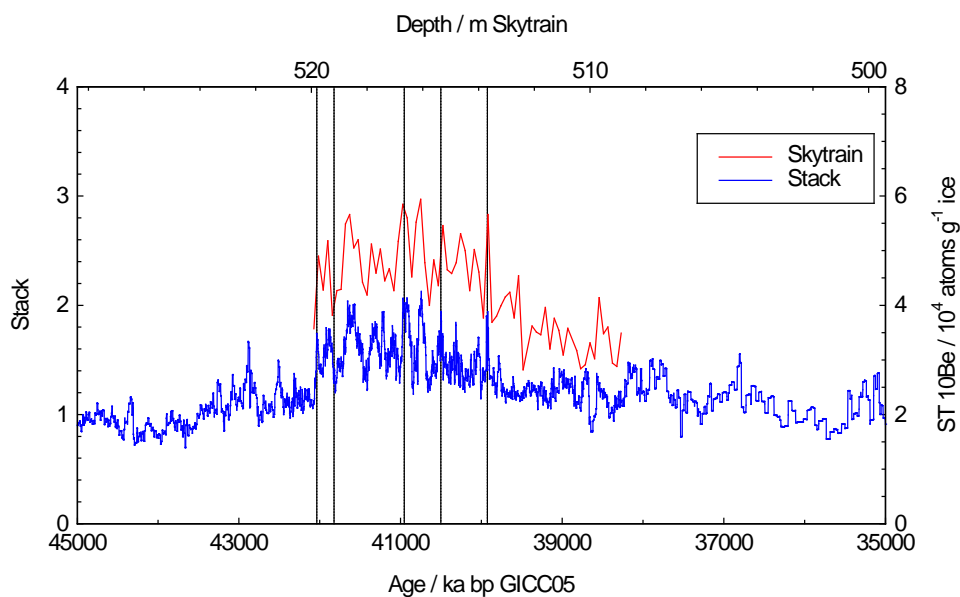


307

308 Figure 5. Methane from Skytrain Ice Rise on the ST22 age scale, along with reference data. Skytrain is
309 shown in purple (continuous is a line, discrete data as dots). In black is a spline of Antarctic data
310 (Köhler et al., 2017). WAIS Divide is shown in yellow (Buizert et al., 2015; Mitchell et al., 2013). Ages
311 shown here are AICC2012. Gas age tie points are shown along the bottom of the figure. The grey
312 shaded area represents the ice (605-617m) with unreliable ages due to flow disturbance (see section
313 9).

314 6.2. ^{10}Be across the Laschamp Event

315 In Fig. 6 we show the Skytrain ^{10}Be concentration from 509-520 m, aligned with the reference
316 dataset. The common shape across the wider event as well as the presence of individual peaks and
317 troughs is clear. We chose 5 tie points in the range 39.9-42.0 ka bp (Table S4).



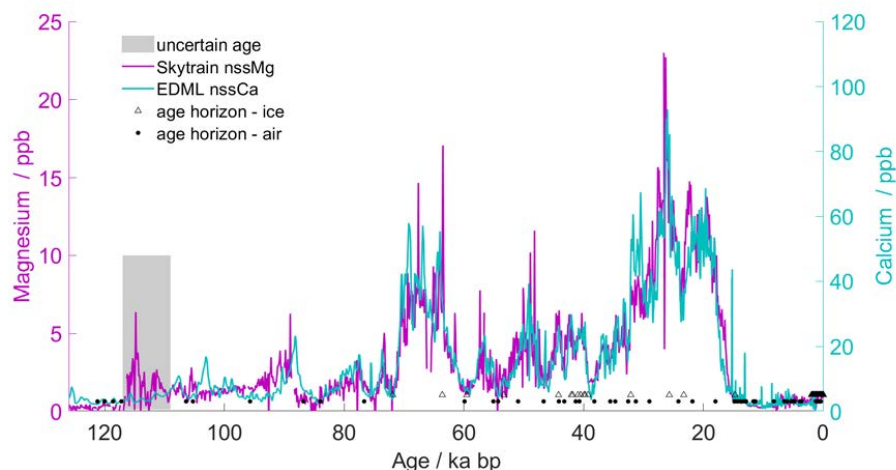
318

319 Figure 6. ^{10}Be concentration in the Skytrain (ST) ice core (red) compared to the normalised stack of
320 ice core radionuclide data (Adolphi et al., 2018). Two samples with obvious low outlier
321 concentrations in the ST record have not been plotted. Vertical lines show the tie points used in this
322 study.

323 6.3. nssMg compared to Ca at EDML

324 Skytrain nssMg was compared to nssCa from EDML (Fischer et al., 2007) (Fig. 7). The two records
325 show strong similarities, as does Skytrain Al (not shown) where it exceeds the detection limit;
326 comparison with EDC nssCa (Wolff et al., 2010) shows a comparably good match. We chose a few
327 obvious tie points (Table S4) concentrating on regions with clear variability and trying to fill the gaps
328 where fewer ice tie points existed. We discuss the ice below 100 ka in section 7.

329



330

331 Figure 7. nssMg at Skytrain shown on its age scale after synchronisation (purple). nssCa from EDML
332 (cyan) (Fischer et al., 2007). Tie points used in this paper are shown (circles are gas age, triangles are
333 ice age ties). The grey shaded area represents the ice (605-617m) with unreliable ages due to flow
334 disturbance (see section 9).

335 7. Dating the ice older than 100 ka

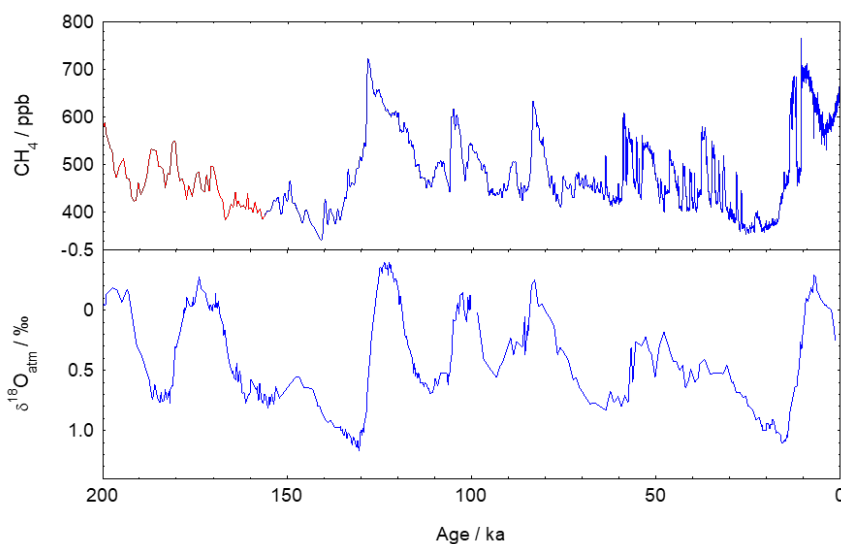
336 Below about 600 m (100 ka), methane continues to show a pattern similar to that of the reference
337 record, with a peak between 600-603 m (Fig. 3) that seems to correspond to the methane peak
338 associated with Greenland interstadial (GI) 24 at 102-107 ka (Baumgartner et al., 2014; Capron et al.,
339 2010). However below this, between 605-608 m, there is a further methane peak that appears
340 anomalous: its concentrations are too high to match the reference data at GI 25. Whereas methane
341 peaks typically have a sharp jump in concentration at their old (deeper) side, this peak has a sharp
342 drop at its shallower side. From 616 to 622 m, methane rises in a stepped fashion similar to the
343 increase seen in the reference record on the young side of the LIG between 114 and 123 ka, before
344 plateauing (~625-629 m) at concentrations typical of the last interglacial (as confirmed by the
345 discrete measurements made in Bern, with several concentrations between 630 and 644 ppb).
346 However there are no values (in either the continuous or discrete data) that reach those (going
347 above 700 ppb) that are seen in the reference data in the early last interglacial peak between 127
348 and 129 ka. Additionally, methane experiences a rapid alternation of values (two values > 600 ppb
349 surrounding a value of 400 ppb within a metre) at 631 m (the base of the values that appear to be
350 interglacial). This coincides (in depth) with a rapid alternation in water isotope ratios (not shown
351 here). Finally there are also very few values below 400 ppb that would correspond to the low values
352 seen in the reference data during the penultimate glacial maximum between about 140-145 ka.



353 These observations suggest that the ice is in good chronological order to 107 ka and probably from
354 about 117-126 ka, but that there might be a flow disturbance between 107 and 117 ka, and a
355 definite disturbance and discontinuity at the base of the last interglacial ice with some thousands of
356 years potentially missing from our record. Later we speculate on the reasons for this. For now it
357 causes us to be concerned about the integrity of the record above this depth (ie the LIG to 126 ka). It
358 suggests that the use of simple pattern matching of methane and nssMg in the LIG ice might risk a
359 false assignment, and so instead we seek a more definite quantitative match.

360 7.1. CH₄ and δ¹⁸O_{atm}

361 Flow disturbances affecting LIG ice have been seen previously, though until now this has been
362 observed mainly in Greenland. To confirm the age of ice with difficult stratigraphy, and even to re-
363 order disordered layers, previous authors have used a combination of methane and δ¹⁸O_{atm}
364 (Chappellaz et al., 1997; NEEM Community Members, 2013; Yau et al., 2016). Provided data are
365 sufficiently precise, the two-dimensional field of these parameters can define an age for a given
366 layer that is close to unique within the plausible range. In Fig. 8 we show the reference data for CH₄
367 and δ¹⁸O_{atm}.



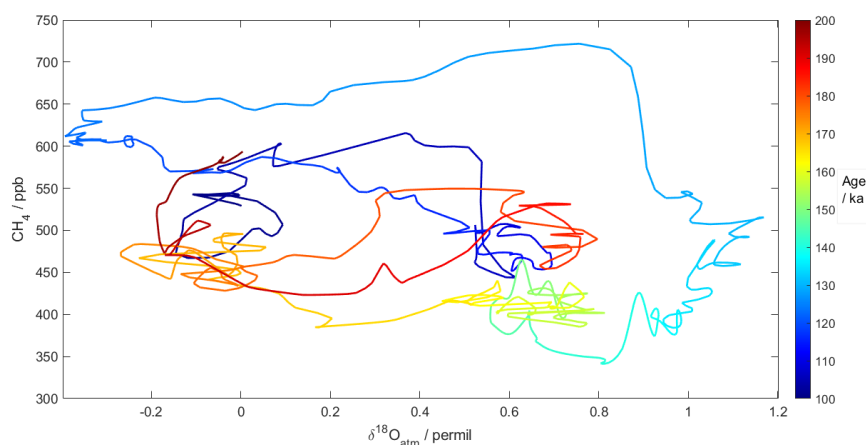
368

369 Figure 8. Reference data for CH₄, to 156 ka in blue (Köhler et al., 2017), beyond 156 ka in red
370 (Loulergue et al., 2008) and δ¹⁸O_{atm} (Extier et al., 2018) over the last 200 ka. Data are all on the
371 AICC2012 age model.

372



373 By plotting the two-dimensional distribution of values (Fig. 9) one can see how the data clearly
374 differentiate samples of different ages – this is particularly true in the section from about 120-150 ka
375 (section that goes clockwise in increasing age from mid-blue to green). While the $\delta^{18}\text{O}_{\text{atm}}$ data were
376 used mainly in combination with CH_4 to assess the ages of ice around the LIG, $\delta^{18}\text{O}_{\text{atm}}$ was also
377 measured in two Skytrain ice core samples from the Holocene and two from the last glacial
378 maximum: these were not used to construct the age scale but the values were entirely consistent
379 with the modelled ages. Three samples were also measured between 435 and 456 m. These three
380 values of $\delta^{18}\text{O}_{\text{atm}}$, along with the less precise CH_4 data obtained from the continuous measurements,
381 were used to assign ages (Table S1) more precisely between 11 and 15 ka in a section in which
382 $\delta^{18}\text{O}_{\text{atm}}$ is increasing rapidly with age (Fig. 8).



383
384 Figure 9. Cross plot of CH_4 (Köhler et al., 2017; Louergue et al., 2008) and $\delta^{18}\text{O}_{\text{atm}}$ (Extier et al., 2018)
385 reference data for the period 100-200 ka. The colourbar indicates the age of the sample.

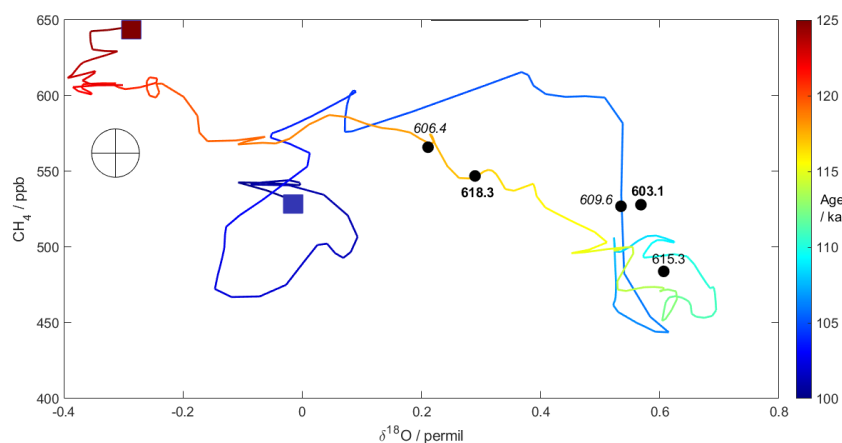
386

387 Twenty Skytrain ice core samples were analysed for $\delta^{18}\text{O}_{\text{atm}}$ between 600 and 635 m depth, covering
388 the period that the discussion above would lead us to expect is older than 100 ka. In all but two
389 cases discrete methane measurements were made (in Bern) on an adjacent sample (a few cm away
390 from the $\delta^{18}\text{O}_{\text{atm}}$ sample).

391 We now examine the data at depths for which we have both $\delta^{18}\text{O}_{\text{atm}}$ and methane measurements.
392 We start with the data from 603-618 m (Fig. 10). The data point at 603.1 m can be assigned an age of
393 ~ 106 ka, as we had already deduced above from the shape and amplitude of the methane peak
394 alone. While the point at 606.4 m matches best with ~ 118 ka, the 3 data points deeper than that

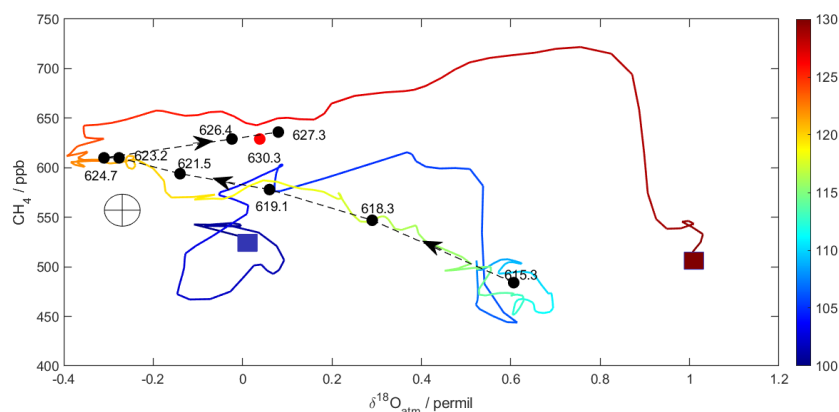


395 (609-618 m) are only compatible with younger ages, between 106 and 117 ka. We cannot untangle
396 this section but there is apparently some degree of disturbance at least between 605 and 615 m.
397 Turning now to Fig. 11, the data from 615.3 to 627.3 m plot in chronological sequence with respect
398 to the reference data between about 110-126 ka. Most of these points are not consistent with
399 $\delta^{18}\text{O}_{\text{atm}}$ and methane values at any other ages in the range, 60-180 ka. Crucially the two datapoints
400 at 623.2 and 624.7 m with very negative $\delta^{18}\text{O}_{\text{atm}}$ and $\text{CH}_4 > 600$ ppb are not compatible with any other
401 age in the past 200 kyr other than the LIG at around 122 ka, and a short period in the Holocene at 7
402 ka. These datapoints are also incompatible with any mixtures of ice from other depths. Because the
403 data point at 615.3 m is compatible with a range of ages, we choose a conservative range of depths
404 from 617 m (just above the clear match at 618.3 m) to 628 m where we are very confident that we
405 have a sequence of ice from the last interglacial, covering the period 126 ka to 117 ka. Although it
406 lies within the uncertainty of the values at 627.3 m, the data point at 630.3 m (shown in red) is also
407 only consistent with the last interglacial, but does not show the expected increase in age with depth,
408 and could show a reversal in age. As this is already in the section that appears disturbed in methane
409 and $\delta^{18}\text{O}_{\text{ice}}$, we consider this data point and the ice around it as subject to disturbance.



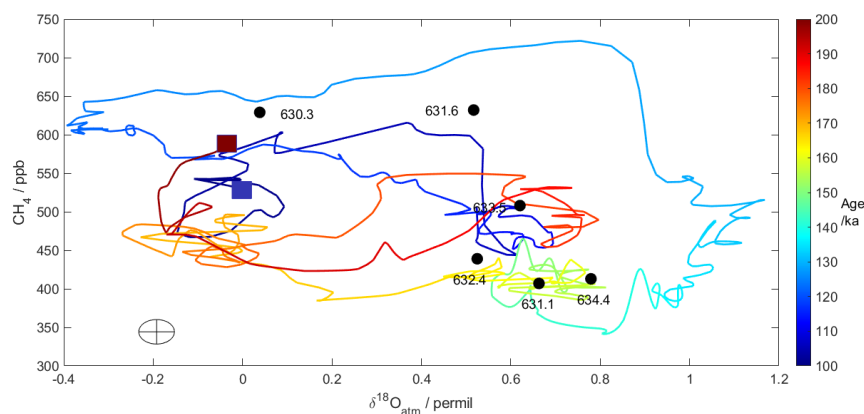
410

411 Figure 10. Cross plot of CH_4 (Köhler et al., 2017) and $\delta^{18}\text{O}_{\text{atm}}$ (Extier et al., 2018) reference data for
412 the period 100-125 ka, along with Skytrain Ice Rise data from 603-618 m depth (black dots). The
413 combined uncertainty (used to decide whether a match between the Skytrain and reference data is
414 acceptable) is shown by the grey ellipse/cross. The start (125 ka) and end (100 ka) of the reference
415 curve are marked by red and blue squares. Skytrain data points are marked with depths; the ones
416 we later judge as being in disturbed ice are marked with italics, while the ones we consider well-
417 dated are in bold.



418
419 Figure 11. Cross plot of CH_4 (Köhler et al., 2017) and $\delta^{18}\text{O}_{\text{atm}}$ (Extier et al., 2018) reference data for
420 the period, 100-130 ka, along with Skytrain Ice Rise data from 615-628 m depth (black dots joined by
421 dashed line with arrows pointing in order of increasing depth) and 630.3 m (red dot). The combined
422 uncertainty (used to decide whether a match between the Skytrain and reference data is acceptable)
423 is shown by the grey ellipse/cross. The start (130 ka) and end (100 ka) of the reference curve are
424 marked by red and blue squares.

425
426 Finally, we examine the data from 630 m to 635 m (Fig. 12). The point at 631.6, sitting close to
427 clearly disturbed ice with rapidly changing values of CH_4 and $\delta^{18}\text{O}_{\text{ice}}$, has values not seen in the
428 reference data, and is probably a mixture of interglacial and glacial ice. The other data have values
429 consistent with ages that would occur in the middle of MIS6 (140-180 ka), or alternatively could
430 originate from ice that is much older (from an earlier glacial cycle). Because there are a number of
431 age solutions within the uncertainty of the measurements we do not attempt to assign ages to these
432 data points.



433



434 Figure 12. Cross plot of CH₄ (Köhler et al., 2017; Loulergue et al., 2008) and δ¹⁸O_{atm} (Extier et al.,
435 2018) reference data for the period 100-200 ka. The colourbar indicates the age of the sample. Also
436 shown are the Skytrain data from 630 m downwards (black dots). The combined uncertainty (used to
437 decide whether a match between the Skytrain and reference data is acceptable) is shown by the
438 grey ellipse/cross. The start (200 ka) and end (100 ka) of the reference curve are marked by red and
439 blue squares.

440

441 7.2. Stratigraphy around the LIG

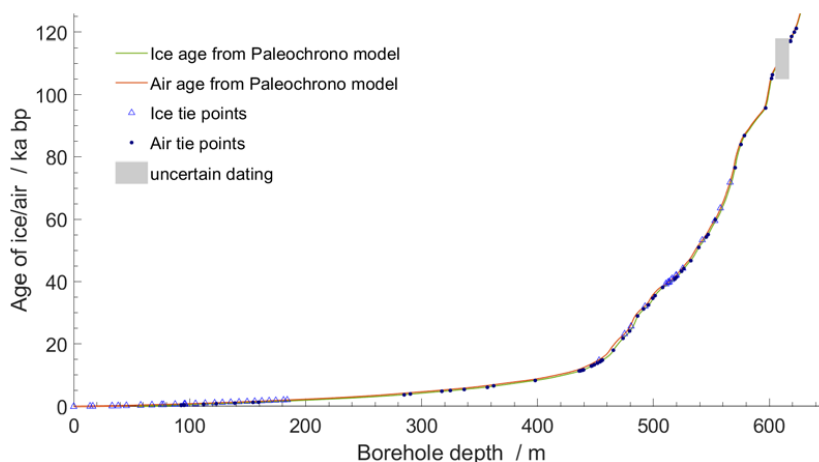
442 Combining the observation that no ice has methane values that fit in the age ranges 127-129 ka or
443 ~140 ka, and the positive identification of ice with unique combinations of CH₄ and δ¹⁸O_{atm}, we
444 conclude the following:

- 445 a) there is probably a flow disturbance at the top of the last interglacial section, with ice from ~106-
446 117 ka repeated;
- 447 b) despite this, there is a continuous section of ice from 617-628 m that represents the time period
448 from 117-126 ka in good order;
- 449 c) there is strongly disturbed ice at the base of the LIG section, with the ice below it most likely
450 representing much older ice from MIS6 or beyond.

451

452 8. Application of Paleochrono

453 The Paleochrono model was run using the prior constraints discussed in section 3 and the tie points
454 described in sections 6 (and shown in Table S3 and S4). For the section deeper than 600 m we have
455 assigned tie points based on CH₄ and δ¹⁸O_{atm} that anchor 603 m at 106 ka, and ties for each
456 CH₄/δ¹⁸O_{atm} pair between 617 and 628 m (117-126 ka). We then assigned a much older age to 632 m
457 just to allow continuity of the age scale to the bed. No other tie points were applied below 628 m
458 (126 ka), and the ice ages below that were ignored. Between the tie points at 603 and 618 m,
459 Paleochrono assigns ages but because we know that there is disturbance and likely repeated ice, we
460 cannot trust all of them. As a compromise, in our age scale we report the ages as far as 605 m (108.7
461 ka) and from 617 m (~117 ka) but do not show any ages for 605-617 m. The age model is reported
462 with both ice age and gas age, along with uncertainties derived from the model. Fig. 13 shows the
463 depth-age relationship (continuous line) from the model. A depth-age lookup table is supplied in the
464 supplement. Methane and nssMg data are shown on the derived age model to 126 ka in Figs. 5 and
465 7. We have placed a grey bar on data in the disturbed section (605-617 m) where ages cannot be
466 considered reliable.

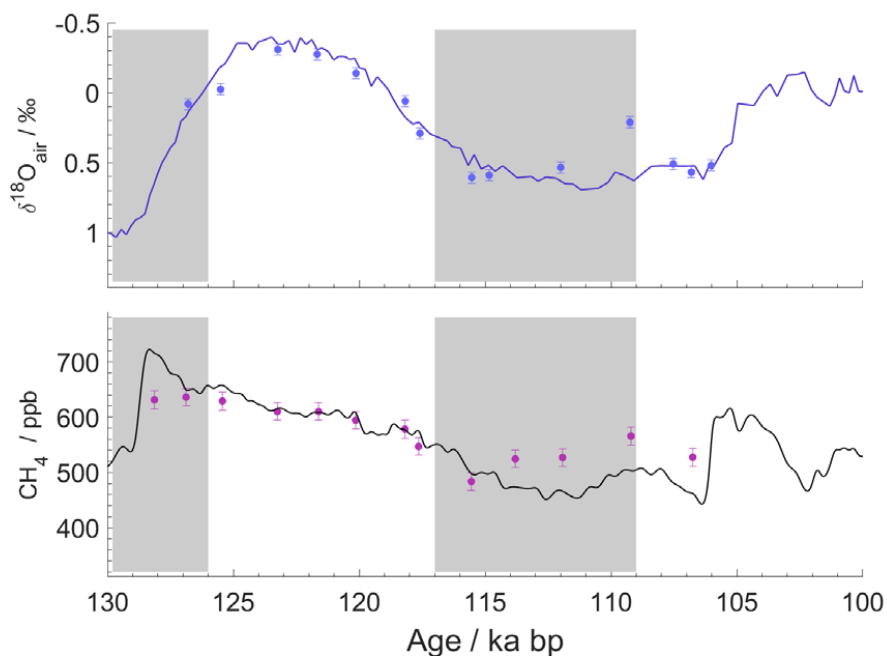


467

468 Figure 13. Age against depth for the Skytrain Ice Rise ice core. Ice and air age are shown, along with
469 the tie points we applied. The section with unreliable ages (605-617 m) is greyed out.

470 In the supplement we present the deposition rate (Fig S1) and thinning function (Fig. S2) derived
471 from the model. No dramatic deviations are seen, indicating that the derived age model is physically
472 reasonable. However given the flow disturbances beyond 605 m the derived deposition rate and
473 thinning may be unreliable from 605 m to the bed.

474 To further assess the age assignments around the LIG, in Fig. 14 we show the values of discrete
475 measurements of CH_4 and $\delta^{18}\text{O}_{\text{atm}}$ with the ages from Paleochrono for the sections of ice we
476 consider less disturbed. It can be seen that both the values and sequence for both parameters are
477 consistent, and generally match the reference data within uncertainty between 117 and 126 ka.
478 Although Paleochrono separated them in order to maintain continuity, the data points (at 626.4 and
479 627.3 m), showing as slightly displaced from the reference curves at 125 and 127 ka in Fig. 14, were
480 originally both assigned tie point ages of ~ 126 ka, which would also place them on the reference
481 curves.



482

483 Figure 14: Reference data for CH_4 and $\delta^{18}\text{O}_{\text{atm}}$ between 100 and 130 ka (as in Fig. 8), along with
484 discrete measurements (symbols) for the Skytrain Ice Rise ice core. Sections with unreliable ages
485 (605-617 m and >628 m) are greyed out. The error bars are the combined uncertainty (at 1 sigma) of
486 the Skytrain and reference data.

487 9. Disturbed ice around the LIG

488 It is evident that there is ice disturbance both at the top, and particularly at the base, of the LIG.
489 Such disturbances have been observed in previous LIG ice, though until now only documented in
490 Greenland ice (Grootes et al., 1993; NEEM Community Members, 2013). Such discontinuities have
491 been hypothesised to result from the contrast between ice layers with very different rheological
492 properties, due to changes in impurity content and grain size (LIG versus Penultimate Glacial
493 Maximum (PGM) and LIG versus late MIS 5) (NEEM Community Members, 2013). We expect smaller
494 contrasts in properties in Antarctica compared to Greenland. However, a tendency to become
495 disturbed and folded might be exacerbated at Skytrain Ice Rise by the existence of a rather large
496 Raymond arch (Mulvaney et al., 2021), a dynamic feature seen in the radar profiles, extending right
497 to the bed (the internal layering (Mulvaney et al., 2021) shows upwarping of order 50 m within



498 around 1 km horizontal distance only 100 m above the bed). Although we expect Skytrain Ice rise to
499 have remained a separate flow centre, it is likely that the position of the dome was different during
500 the LGM when the Ronne Ice Shelf would have been grounded and provided greater constraint to
501 the north and east; this could also have led to disturbance around the LIG ice which would already
502 have been deep in the ice column at that time.

503 We consider here possible alternative causes for the hiatus, with ice from 127-129 ka missing from
504 our sequence, and probably ice from 129 to at least 140 ka also unrepresented.

- 505 a) The first possibility is that there was no snow accumulation during this period. This is
506 considered extremely unlikely. The section from 127-129 ka at other Antarctic sites shows
507 high temperatures and inferred high accumulation rates.
- 508 b) A second possibility is that the ice from inland overrode Skytrain Ice rise causing some layers
509 to be removed completely. However, the Ellsworth Mountains provide a high and rather
510 solid barrier against such flow. There is also no sign of ice anywhere in the core with the
511 much more negative water isotopic contents one would expect from ice originating at much
512 higher altitude inland.
- 513 c) Some ice sheet models have inferred a possible loss of ice from parts of WAIS during the LIG
514 (DeConto and Pollard, 2016). This hypothesis raises the possibility that ice was completely
515 lost from Skytrain Ice Rise in the warmest part of the LIG. However, the existence of more
516 than 20 m of ice that appears to derive from MIS6 or older suggests that ice was not
517 completely removed from Skytrain Ice rise. In addition if some ice was lost by melting, while
518 older ice was retained, we would expect to see bubble-free ice (caused by refreezing after
519 melting). This is not observed anywhere in the core: normal values of total air content and
520 methane concentrations are seen at all depths.

521 We therefore conclude that the only plausible explanation for our observations is flow
522 disturbance due to contrasting rheology.

523

524 10. Conclusion

525 We have constructed an age model, which we call ST22, for the Skytrain Ice Rise ice core. This age
526 model is based mainly on tie points to previous Antarctic ice cores, using a range of analyses. The
527 age-depth relationship is well-behaved until at least 100 ka. There appears to be flow disturbance at
528 the top of the LIG section, but the core contains ice from the last interglacial (117 to 126 ka) in good



529 stratigraphic order. It is however missing the earliest part of the LIG, and the coldest part of the
530 PGM, apparently also due to flow disturbance affecting ice layers with contrasting rheologies.

531 Because the missing ice appears to have been affected by flow disturbances, we surmise that
532 another core at a suitably chosen location on Skytrain Ice rise might be capable of retrieving ice from
533 the missing sections. This is the first time that flow disturbances around the LIG have been clearly
534 documented for Antarctica, as they have been several times for Greenland. These disturbances raise
535 the possibility that such disturbances might also have affected other records of the LIG (Korotkikh et
536 al., 2011). One obvious conclusion from our data is that the ice sheet was certainly present at
537 Skytrain Ice Rise during the LIG.

538 **Data availability**

539 The continuous methane and nssMg used in this paper (and shown in Figs 5 and 7) have been
540 submitted to Pangaea. The discrete CH₄, δ¹⁸O_{atm} and ¹⁰Be data used in this paper are attached as
541 supplementary data (Tables S1 and S2). The air and ice tie points used in Paleochrono are attached
542 as supplementary data (Tables S3 and S4). All reference data used in this paper are already
543 published and available online. The final derived age model ST22 is attached as supplementary table
544 S5, and has been submitted to Pangaea.

545 **Author contributions**

546 The first two authors contributed equally to this paper. The paper was written by RMul and EW with
547 contributions mainly from HH, MG and RR. The ice core was drilled and sectioned by EW, RMul, CN-
548 A, MG, IR. The CFA analysis was performed by HH, MG, JH, RMul, RR and IR. Discrete methane
549 analyses were provided by LS, HF and TS; δ¹⁸O_{atm} data were provided by FP and AL; ¹⁰Be data were
550 provided by MC and RMus. RMul ran Paleochrono with advice from FP. All authors contributed to
551 improving the final paper.

552 **Competing interests**

553 The authors declare that they have no competing interests.

554 **Acknowledgments**

555 The authors thank Shaun Miller, Charlie Durman, Amy King, Emily Ludlow, Liz Thomas and Victoria
556 Alcock for help with cutting, processing and analysing the ice core. This project has received funding
557 from the European Research Council under the Horizon 2020 research and innovation programme
558 (grant agreement No 742224, WACSWAIN). TS and LS acknowledge funding from the Swiss National
559 Science Foundation (#172745 and #2000492), and all authors from the University of Bern gratefully



560 acknowledge the long-term support of ice core science by the Swiss National Science Foundation.
561 This material reflects only the authors' views and the Commission is not liable for any use that may
562 be made of the information contained therein. EW and HH have also been funded for part of this
563 work through a Royal Society Professorship. The development of PaleoChrono was funded by two
564 CNRS/INSU/LEFE projects called "IceChrono" and "CO2Role".

565 **References**

- 566 Adolphi, F., Bronk Ramsey, C., Erhardt, T., Edwards, R. L., Cheng, H., Turney, C. S. M., Cooper, A.,
567 Svensson, A., Rasmussen, S. O., Fischer, H., and Muscheler, R.: Connecting the Greenland ice-core
568 and U/Th timescales via cosmogenic radionuclides: testing the synchronicity of Dansgaard–Oeschger
569 events, *Clim. Past*, 14, 1755–1781, doi: 10.5194/cp-14-1755-2018, 2018.
- 570
571 Adolphi, F. and Muscheler, R.: Synchronizing the Greenland ice core and radiocarbon timescales over
572 the Holocene – Bayesian wiggle-matching of cosmogenic radionuclide records, *Clim. Past*, 12, 15–30,
573 doi: 10.5194/cp-12-15-2016, 2016.
- 574
575 Ahn, J. and Brook, E. J.: Atmospheric CO₂ and climate on millennial time scales during the last glacial
576 period, *Science*, 322, 83–85, doi: 10.1126/science.1160832, 2008.
- 577
578 Baggenstos, D., Severinghaus, J. P., Mulvaney, R., McConnell, J. R., Sigl, M., Maselli, O., Petit, J. R.,
579 Grente, B., and Steig, E. J.: A Horizontal Ice Core From Taylor Glacier, Its Implications for Antarctic
580 Climate History, and an Improved Taylor Dome Ice Core Time Scale, *Paleoceanography and*
581 *Paleoclimatology*, 33, 778–794, doi: 10.1029/2017pa003297, 2018.
- 582
583 Baumgartner, M., Kindler, P., Eicher, O., Floch, G., Schilt, A., Schwander, J., Spahni, R., Capron, E.,
584 Chappellaz, J., Leuenberger, M., Fischer, H., and Stocker, T. F.: NGRIP CH₄ concentration from 120 to
585 10 kyr before present and its relation to a delta N-15 temperature reconstruction from the same ice
586 core, *Climate of the Past*, 10, 903–920, doi: 10.5194/cp-10-903-2014, 2014.
- 587
588 Bazin, L., Landais, A., Lemieux-Dudon, B., Kele, H. T. M., Veres, D., Parrenin, F., Martinerie, P., Ritz, C.,
589 Capron, E., Lipenkov, V., Loutre, M. F., Raynaud, D., Vinther, B., Svensson, A., Rasmussen, S. O.,
590 Severi, M., Blunier, T., Leuenberger, M., Fischer, H., Masson-Delmotte, V., Chappellaz, J., and Wolff,
591 E. W.: An optimised multi-proxy, multi-site Antarctic ice and gas orbital chronology (AICC2012): 120–
592 800 ka, *Climate of the Past*, 9, 1715–1731, 2013.
- 593
594 Brook, E. J., White, J. W. C., Schilla, A. S. M., Bender, M. L., Barnett, B., Severinghaus, J. P., Taylor, K.
595 C., Alley, R. B., and Steig, E. J.: Timing of millennial-scale climate change at Siple Dome, West
596 Antarctica, during the last glacial period, *Quat. Sci. Rev.*, 24, 1333–1343, 2005.
- 597
598 Buizert, C., Cuffey, K. M., Severinghaus, J. P., Baggenstos, D., Fudge, T. J., Steig, E. J., Markle, B. R.,
599 Winstrup, M., Rhodes, R. H., Brook, E. J., Sowers, T. A., Clow, G. D., Cheng, H., Edwards, R. L., Sigl, M.,
600 McConnell, J. R., and Taylor, K. C.: The WAIS Divide deep ice core WD2014 chronology – Part 1:
601 Methane synchronization (68–31 kaBP) and the gas age–ice age difference, *Climate of the Past*, 11,
602 153–173, doi: 10.5194/cp-11-153-2015, 2015.



- 603
604 Buizert, C., Sigl, M., Severi, M., Markle, B. R., Wettstein, J. J., McConnell, J. R., Pedro, J. B.,
605 Sodemann, H., Goto-Azuma, K., Kawamura, K., Fujita, S., Motoyama, H., Hirabayashi, M., Uemura, R.,
606 Stenni, B., Parrenin, F., He, F., Fudge, T. J., and Steig, E. J.: Abrupt ice-age shifts in southern westerly
607 winds and Antarctic climate forced from the north, *Nature*, 563, 681-685, doi: 10.1038/s41586-018-
608 0727-5, 2018.
- 609
610 Capron, E., Landais, A., Lemieux-Dudon, B., Schilt, A., Masson-Delmotte, V., Buiron, D., Chappellaz, J.,
611 Dahl-Jensen, D., Johnsen, S., Leuenberger, M., Loulergue, L., and Oerter, H.: Synchronising EDML and
612 NorthGRIP ice cores using $\delta^{18}\text{O}$ of atmospheric oxygen ($\delta^{18}\text{O}_{\text{atm}}$) and CH_4 measurements over MIS 5
613 (80-123 ka), *Quat. Sci. Rev.*, 29, 222-234, 2010.
- 614
615 Chappellaz, J., Brook, E., Blunier, T., and Malaizé, B.: CH_4 and delta O-18 of O-2 records from
616 Antarctic and Greenland ice: A clue for stratigraphic disturbance in the bottom part of the Greenland
617 Ice Core Project and the Greenland Ice Sheet Project 2 ice cores, *J. Geophys. Res.*, 102, 26547-26557,
618 1997.
- 619
620 Christl, M., Vockenhuber, C., Kubik, P. W., Wacker, L., Lachner, J., Alfimov, V., and Synal, H. A.: The
621 ETH Zurich AMS facilities: Performance parameters and reference materials, *Nuclear Instruments
622 and Methods in Physics Research Section B: Beam Interactions with Materials and Atoms*, 294, 29-
623 38, doi: <https://doi.org/10.1016/j.nimb.2012.03.004>, 2013.
- 624
625 Crotti, I., Landais, A., Stenni, B., Bazin, L., Parrenin, F., Frezzotti, M., Ritterbusch, F., Lu, Z.-T., Jiang,
626 W., Yang, G.-M., Fourné, E., Orsi, A., Jacob, R., Minster, B., Prié, F., Dreossi, G., and Barbante, C.: An
627 extension of the TALDICE ice core age scale reaching back to MIS 10.1, *Quat. Sci. Rev.*, 266, 107078,
628 doi: <https://doi.org/10.1016/j.quascirev.2021.107078>, 2021.
- 629
630 DeConto, R. M. and Pollard, D.: Contribution of Antarctica to past and future sea-level rise, *Nature*,
631 531, 591-597, doi: 10.1038/nature17145, 2016.
- 632
633 DeConto, R. M., Pollard, D., Alley, R. B., Velicogna, I., Gasson, E., Gomez, N., Sadai, S., Condrón, A.,
634 Gilford, D. M., Ashe, E. L., Kopp, R. E., Li, D., and Dutton, A.: The Paris Climate Agreement and future
635 sea-level rise from Antarctica, *Nature*, 593, 83-89, doi: 10.1038/s41586-021-03427-0, 2021.
- 636
637 Dutton, A., Carlson, A. E., Long, A. J., Milne, G. A., Clark, P. U., DeConto, R., Horton, B. P., Rahmstorf,
638 S., and Raymo, M. E.: Sea-level rise due to polar ice-sheet mass loss during past warm periods,
639 *Science*, 349, 153-+, doi: 10.1126/science.aaa4019, 2015.
- 640
641 Dyer, B., Austermann, J., D'Andrea, W. J., Creel, R. C., Sandstrom, M. R., Cashman, M., Rovere, A.,
642 and Raymo, M. E.: Sea-level trends across The Bahamas constrain peak last interglacial ice melt,
643 *Proceedings of the National Academy of Sciences*, 118, e2026839118, doi:
644 10.1073/pnas.2026839118, 2021.
- 645
646 EPICA Community Members: Eight glacial cycles from an Antarctic ice core, *Nature*, 429, 623-628,
647 doi: 10.1038/nature02599, 2004.
- 648



- 649 Epifanio, J. A., Brook, E. J., Buizert, C., Edwards, J. S., Sowers, T. A., Kahle, E. C., Severinghaus, J. P.,
650 Steig, E. J., Winski, D. A., Osterberg, E. C., Fudge, T. J., Aydin, M., Hood, E., Kalk, M., Kreutz, K. J.,
651 Ferris, D. G., and Kennedy, J. A.: The SP19 chronology for the South Pole Ice Core – Part 2: gas
652 chronology, Δ age, and smoothing of atmospheric records, *Clim. Past*, 16, 2431-2444, doi:
653 10.5194/cp-16-2431-2020, 2020.
- 654
655 Extier, T., Landais, A., Bréant, C., Prié, F., Bazin, L., Dreyfus, G., Roche, D. M., and Leuenberger, M.:
656 On the use of $\delta^{18}\text{O}_{\text{atm}}$ for ice core dating, *Quat. Sci. Rev.*, 185, 244-257, doi:
657 <https://doi.org/10.1016/j.quascirev.2018.02.008>, 2018.
- 658
659 Fischer, H., Fundel, F., Ruth, U., Twarloh, B., Wegner, A., Udisti, R., Becagli, S., Castellano, E.,
660 Morganti, A., Severi, M., Wolff, E. W., Littot, G. C., Rothlisberger, R., Mulvaney, R., Hutterli, M. A.,
661 Kaufmann, P., Federer, U., Lambert, F., Bigler, M., Hansson, M., Jonsell, U., de Angelis, M., Gabrielli,
662 P., Boutron, C., Siggaard-Andersen, M. L., Steffensen, J. P., Barbante, C., Gaspari, V., and Wagenbach,
663 D.: Reconstruction of millennial changes in transport, dust emission and regional differences in sea
664 ice coverage using the deep EPICA ice cores from the Atlantic and Indian Ocean sector of Antarctica.,
665 *Earth planet. Sci. Lett.*, 260, 340-354, 2007.
- 666
667 Fox-Kemper, B., Hewitt, H., Xiao, C., Aðalgeirsdóttir, G., Drijfhout, S. S., Edwards, T. L., Golledge, N.
668 R., Hemer, M., Kopp, R. E., Krinner, G., Mix, A., Notz, D., Nowicki, S., Nurhati, I. S., Ruiz, L., Sallée, J.-
669 B., Slangen, A. B. A., and Yu, Y.: Chapter 9: Ocean, Cryosphere and Sea Level Change. In: *Climate*
670 *Change 2021: The Physical Science Basis. Contribution of Working Group I to the Sixth Assessment*
671 *Report of the Intergovernmental Panel on Climate Change*, Masson-Delmotte, V., Zhai, P., Pirani, A.,
672 Connors, S. L., Péan, C., Berger, S., Caud, N., Chen, Y., Goldfarb, L., Gomis, M. I., Huang, M., Leitzell,
673 K., Lonnoy, E., Matthews, J. B. R., Maycock, T. K., Waterfield, T., Yelekçi, O., Yu, R., and Zhou, B.
674 (Eds.), Cambridge University Press, 2021.
- 675
676 Gilford, D. M., Ashe, E. L., DeConto, R. M., Kopp, R. E., Pollard, D., and Rovere, A.: Could the Last
677 Interglacial Constrain Projections of Future Antarctic Ice Mass Loss and Sea-Level Rise?, *Journal of*
678 *Geophysical Research: Earth Surface*, 125, e2019JF005418, doi:
679 <https://doi.org/10.1029/2019JF005418>, 2020.
- 680
681 Grieman, M. M., Hoffmann, H. M., Humby, J. D., Mulvaney, R., Nehrbass-Ahles, C., Rix, J., Thomas, E.
682 R., Tuckwell, R., and Wolff, E. W.: Continuous flow analysis methods for sodium, magnesium and
683 calcium detection in the Skytrain ice core, *J. Glaciol.*, 68, 90-100, doi: 10.1017/jog.2021.75, 2021.
- 684
685 Grootes, P. M., Steig, E. J., Stuiver, M., Waddington, E. D., and Morse, D. L.: The Taylor dome
686 antarctic O-18 record and globally synchronous changes in climate, *Quaternary Res.*, 56, 289-298,
687 2001.
- 688
689 Grootes, P. M., Stuiver, M., White, J. W. C., Johnsen, S., and Jouzel, J.: Comparison of oxygen isotope
690 records from the GISP2 and GRIP Greenland ice cores, *Nature*, 366, 552-554, 1993.
- 691
692 Hoffmann, H. M., Grieman, M. M., King, A. C. F., Epifanio, J. A., Martin, K., Vladimirova, D., Pryer, H.
693 V., Doyle, E., Schmidt, A., Humby, J. D., Rowell, I. F., Nehrbass-Ahles, C., Thomas, E. R., Mulvaney, R.,
694 and Wolff, E. W.: The ST22 chronology for the Skytrain Ice Rise ice core – Part 1: A stratigraphic
695 chronology of the last 2000 years, *Clim. Past*, 18, 1831-1847, doi: 10.5194/cp-18-1831-2022, 2022.



- 696
697 Jacobel, R. W., Welch, B. C., Steig, E. J., and Schneider, D. P.: Glaciological and climatic significance of
698 Hercules Dome, Antarctica: An optimal site for deep ice core drilling, *J. Geophys. Res.-Earth Surf.*,
699 110, doi: 10.1029/2004jf000188, 2005.
- 700
701 Kawamura, K., Parrenin, F., Lisiecki, L., Uemura, R., Vimeux, F., Severinghaus, J. P., Hutterli, M. A.,
702 Nakazawa, T., Aoki, S., Jouzel, J., Raymo, M. E., Matsumoto, K., Nakata, H., Motoyama, H., Fujita, S.,
703 Azuma, K., Fujii, Y., and Watanabe, O.: Northern Hemisphere forcing of climatic cycles over the past
704 360,000 years implied by accurately dated Antarctic ice cores, *Nature*, 448, 912-916, 2007.
- 705
706 Köhler, P., Nehrbass-Ahles, C., Schmitt, J., Stocker, T. F., and Fischer, H.: A 156 kyr smoothed history
707 of the atmospheric greenhouse gases CO₂, CH₄, and N₂O and their radiative forcing, *Earth Syst. Sci.*
708 *Data*, 9, 363-387, doi: 10.5194/essd-9-363-2017, 2017.
- 709
710 Korotkikh, E. V., Mayewski, P. A., Handley, M. J., Sneed, S. B., Introne, D. S., Kurbatov, A. V., Dunbar,
711 N. W., and McIntosh, W. C.: The last interglacial as represented in the glaciochemical record from
712 Mount Moulton Blue Ice Area, West Antarctica, *Quat. Sci. Rev.*, 30, 1940-1947, 2011.
- 713
714 Lee, J. E., Brook, E. J., Bertler, N. A. N., Buizert, C., Baisden, T., Blunier, T., Ciobanu, V. G., Conway, H.,
715 Dahl-Jensen, D., Fudge, T. J., Hindmarsh, R., Keller, E. D., Parrenin, F., Severinghaus, J. P., Vallelonga,
716 P., Waddington, E. D., and Winstrup, M.: An 83000-year-old ice core from Roosevelt Island, Ross Sea,
717 Antarctica, *Clim. Past*, 16, 1691-1713, doi: 10.5194/cp-16-1691-2020, 2020.
- 718
719 Loulergue, L., Schilt, A., Spahni, R., Masson-Delmotte, V., Blunier, T., Lemieux, B., Barnola, J. M.,
720 Raynaud, D., Stocker, T. F., and Chappellaz, J.: Orbital and millennial-scale features of atmospheric
721 CH₄ over the last 800,000 years, *Nature*, 453, 383-386, 2008.
- 722
723 Matsuoka, K., Skoglund, A., Roth, G., de Pomereu, J., Griffiths, H., Headland, R., Herried, B.,
724 Katsumata, K., Le Brocq, A., Licht, K., Morgan, F., Neff, P. D., Ritz, C., Scheinert, M., Tamura, T., Van
725 de Putte, A., van den Broeke, M., von Deschanden, A., Deschamps-Berger, C., Van Liefferinge, B.,
726 Tronstad, S., and Melvær, Y.: Quantarctica, an integrated mapping environment for Antarctica, the
727 Southern Ocean, and sub-Antarctic islands, *Environmental Modelling & Software*, 140, 105015, doi:
728 <https://doi.org/10.1016/j.envsoft.2021.105015>, 2021.
- 729
730 Mitchell, L., Brook, E., Lee, J. E., Buizert, C., and Sowers, T.: Constraints on the Late Holocene
731 Anthropogenic Contribution to the Atmospheric Methane Budget, *Science*, 342, 964-966, doi:
732 10.1126/science.1238920, 2013.
- 733
734 Mulvaney, R., Alemany, O., and Possenti, P.: The Berkner Island ice core drilling project, *Ann.*
735 *Glaciol.*, 47, 115-124, 2007.
- 736
737 Mulvaney, R., Rix, J., Polfrey, S., Grieman, M., Martin, C., Nehrbass-Ahles, C., Rowell, I., Tuckwell, R.,
738 and Wolff, E.: Ice drilling on Skytrain Ice Rise and Sherman Island, Antarctica, *Ann. Glaciol.*, 62, 311-
739 323, doi: 10.1017/aog.2021.7, 2021.
- 740



- 741 Mulvaney, R., Röthlisberger, R., Wolff, E. W., Sommer, S., Schwander, J., Hutterli, M. A., and Jouzel,
742 J.: The transition from the last glacial period in inland and near-coastal Antarctica, *Geophys. Res.*
743 *Let.*, 27, 2673-2676, 2000.
- 744
745 Mulvaney, R., Triest, J., and Alemany, O.: The James Ross Island and the Fletcher Promontory ice-
746 core drilling projects, *Ann. Glaciol.*, 55, 179-188, doi: 10.3189/2014AoG68A044, 2014.
- 747
748 NEEM Community Members: Eemian interglacial reconstructed from a Greenland folded ice core
749 *Nature*, 493, 489-494, doi: 10.1038/nature11789, 2013.
- 750
751 Parrenin, F., Bazin, L., Capron, E., Landais, A., Lemieux-Dudon, B., and Masson-Delmotte, V.:
752 IceChrono1: a probabilistic model to compute a common and optimal chronology for several ice
753 cores, *Geosci. Model Dev.*, 8, 1473-1492, doi: 10.5194/gmd-8-1473-2015, 2015.
- 754
755 Raisbeck, G. M., Cauquoin, A., Jouzel, J., Landais, A., Petit, J. R., Lipenkov, V. Y., Beer, J., Synal, H. A.,
756 Oerter, H., Johnsen, S. J., Steffensen, J. P., Svensson, A., and Yiou, F.: An improved north-south
757 synchronization of ice core records around the 41 kyr 10Be peak, *Clim. Past*, 13, 217-229, doi:
758 10.5194/cp-13-217-2017, 2017.
- 759
760 Rhodes, R. H., Brook, E. J., Chiang, J. C. H., Blunier, T., Maselli, O. J., McConnell, J. R., Romanini, D.,
761 and Severinghaus, J. P.: Enhanced tropical methane production in response to iceberg discharge in
762 the North Atlantic, *Science*, 348, 1016-1019, doi: 10.1126/science.1262005, 2015.
- 763
764 Rhodes, R. H., Brook, E. J., McConnell, J. R., Blunier, T., Sime, L. C., Faïn, X., and Mulvaney, R.:
765 Atmospheric methane variability: Centennial-scale signals in the Last Glacial Period, *Global*
766 *Biogeochemical Cycles*, 31, 575-590, doi: 10.1002/2016GB005570, 2017.
- 767
768 Röthlisberger, R., Mulvaney, R., Wolff, E. W., Hutterli, M., Bigler, M., Sommer, S., and Jouzel, J.: Dust
769 and sea salt variability in central East Antarctica (Dome C) over the last 45 kyrs and its implications
770 for southern high-latitude climate, *Geophys. Res. Lett.*, 29, 1963, doi: 10.1029/2002GL015186,
771 2002.
- 772
773 Saltzman, E. S., Dioumaeva, I., and Finley, B. D.: Glacial/interglacial variations in methanesulfonate
774 (MSA) in the Siple Dome ice core, West Antarctica, *Geophys. Res. Lett.*, 33, 2006.
- 775
776 Schmidely, L., Nehrbass-Ahles, C., Schmitt, J., Han, J., Silva, L., Shin, J., Joos, F., Chappellaz, J., Fischer,
777 H., and Stocker, T. F.: CH₄ and N₂O fluctuations during the penultimate deglaciation, *Clim. Past*, 17,
778 1627-1643, doi: 10.5194/cp-17-1627-2021, 2021.
- 779
780 Sigl, M., Fudge, T. J., Winstrup, M., Cole-Dai, J., Ferris, D., McConnell, J. R., Taylor, K. C., Welten, K. C.,
781 Woodruff, T. E., Adolphi, F., Bisiaux, M., Brook, E. J., Buizert, C., Caffee, M. W., Dunbar, N. W.,
782 Edwards, R., Geng, L., Iverson, N., Koffman, B., Layman, L., Maselli, O. J., McGwire, K., Muscheler, R.,
783 Nishiizumi, K., Pasteris, D. R., Rhodes, R. H., and Sowers, T. A.: The WAIS Divide deep ice core
784 WD2014 chronology – Part 2: Annual-layer counting (0–31 ka BP), *Clim. Past*, 12, 769-786, doi:
785 10.5194/cp-12-769-2016, 2016.



786
787 Sigl, M., Toohey, M., McConnell, J. R., Cole-Dai, J., and Severi, M.: Volcanic stratospheric sulfur
788 injections and aerosol optical depth during the Holocene (past 11,500 years) from a bipolar ice core
789 array, *Earth Syst. Sci. Data Discuss.*, 2022, 1-45, doi: 10.5194/essd-2021-422, 2022.

790
791 Veres, D., Bazin, L., Landais, A., Kele, H. T. M., Lemieux-Dudon, B., Parrenin, F., Martinerie, P., Blayo,
792 E., Blunier, T., Capron, E., Chappellaz, J., Rasmussen, S. O., Severi, M., Svensson, A., Vinther, B., and
793 Wolff, E. W.: The Antarctic ice core chronology (AICC2012): an optimised multi-parameter and multi-
794 site dating approach for the last 120 thousand years, *Climate of the Past*, 9, 1733-1748, 2013.

795
796 Wolff, E. W., Barbante, C., Becagli, S., Bigler, M., Boutron, C. F., Castellano, E., De Angelis, M.,
797 Federer, U., Fischer, H., Fundel, F., Hansson, M., Hutterli, M., Jonsell, U., Karlin, T., Kaufmann, P.,
798 Lambert, F., Littot, G. C., Mulvaney, R., Rothlisberger, R., Ruth, U., Severi, M., Siggaard-Andersen, M.
799 L., Sime, L. C., Steffensen, J. P., Stocker, T. F., Traversi, R., Twarloh, B., Udisti, R., Wagenbach, D., and
800 Wegner, A.: Changes in environment over the last 800,000 years from chemical analysis of the EPICA
801 Dome C ice core, *Quat. Sci. Rev.*, 29, 285-295, doi: 10.1016/j.quascirev.2009.06.013, 2010.

802
803 Yau, A. M., Bender, M. L., Robinson, A., and Brook, E. J.: Reconstructing the last interglacial at
804 Summit, Greenland: Insights from GISP2, *Proc. Natl. Acad. Sci. U. S. A.*, 113, 9710-9715, doi:
805 10.1073/pnas.1524766113, 2016.

806
807